

Interacting line-node semimetal and spontaneous symmetry breaking

Bitan Roy

Condensed Matter Theory Center and Joint Quantum Institute,
University of Maryland, College Park, Maryland 20742-4111, USA

(Dated: December 9, 2024)

The effects of short-range electronic interactions in a three dimensional line-node semimetal that supports linearly dispersing quasiparticles around an isolated closed loop in the Brillouin zone are discussed. Due to vanishing density of states various orderings in the bulk of the system, such as the antiferromagnet and charge-density-wave, set in for sufficiently strong onsite (U) and nearest-neighbor (V) repulsions, respectively. While onset of these two orderings from the semimetallic phase takes place through continuous quantum phase transitions, a first order transition separates two ordered phases. By contrast, topologically protected drumhead shaped surface states can undergo charge or spin orderings, depending on relative strength of U and V , even when they are sufficiently weak. Such surface orderings as well as weak long range Coulomb interaction can be conducive to spontaneous symmetry breaking in the bulk for weaker interactions. We also discuss possible superconducting phases and internal symmetry among various orders in this system.

Introduction: The mechanism of mass generation of elementary particles through spontaneous symmetry breaking nowadays leaving the territory of high energy physics curves its path through the fertile ground of condensed matter physics, where a myriad of gapless phases is realized at low energies from complex band structures in solids. A celebrated example of such mass generation is the *superconductivity*, through which gapless excitations residing in the proximity to the Fermi surface acquire *Majorana mass* [1].

Often the energy landscape available for electrons, offered by the periodic potential accommodated by immobile ions, displays band touching only at high symmetry points in the Brillouin zone and gives rise to semimetallic phase when the chemical potential is pinned at band touching point [2]. Although such band touching is usually protected by underlying symmetries, a plethora of broken symmetry phases (BSPs), lacking discrete and/or continuous symmetries, can be realized when electronic interactions are taken into account. We here focus on a three dimensional system that supports linearly dispersing gapless excitations around an isolated two dimensional *loop* in the reciprocal space, the *line-node semimetal* (LNSM), and address the effects of short-range electronic interactions on such unconventional phase of matter. Recently developing interest in LNSM [3–10], along with its possible realization in various materials [11–28], where the strength of electronic interactions varies over a wide range, besides fundamental importance also endows timeliness to this quest.

Due to *linearly* vanishing density of states (DOS) [29], any sufficiently weak local four-fermion interaction (Hubbard-like) is an *irrelevant* perturbation in a three dimensional LNSM. However, beyond a critical strength of interaction various BSPs can set in through continuous quantum phase transitions (QPTs). We identify the antiferromagnet (AF) and charge-density-wave (CDW) as the favorable BSPs among the possible candidates that,

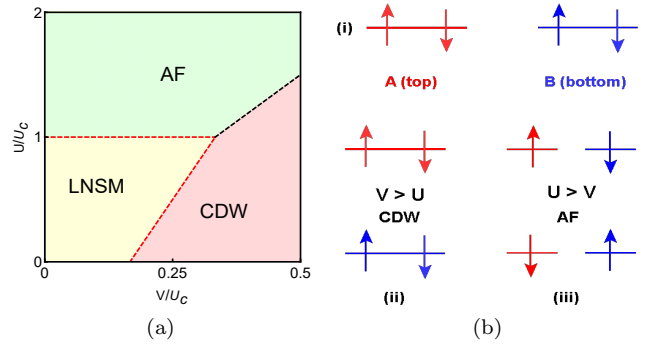


FIG. 1: (Color online) (a) Mean field phase diagram for a three dimensional line-node semimetal (LNSM). Here, U and V respectively corresponds to onsite and nearest-neighbor repulsions, and supports antiferromagnet (AF) and charge-density-wave (CDW) phases, when sufficiently strong. Critical strengths for AF ordering when $V = 0$ is denoted by U_c . Transition(s) across the black (red) dashed line(s) is (are) first order (continuous). (b) (i) Spin degenerate surface states, localized on complimentary sublattices on opposite faces along (001) direction. Two possible splitting for flat surface states: (ii) when $V > U$ and (iii) $U > V$. The surface ordering ordering sets in for infinitesimal strength of U and V , which in turn can trigger corresponding orderings in the bulk for weaker interactions, through *proximity* effect.

for example, can be realized for sufficiently strong onsite Hubbard (U) and nearest-neighbor (V) repulsions, respectively; see Fig. 1(a). The LNSM also supports topologically protected flat *drumhead* shaped surface states, which are susceptible to charge or spin orderings even for infinitesimal interaction; see Fig. 1(b). In turn the surface orderings can induce aforementioned orderings in the bulk through *proximity effect* even at weaker interactions. Thus surface induced ordering in the bulk stands as an experimentally feasible way to induce BSPs in the bulk, as well as drive the system through QPTs by systematically tuning the thickness of the sample [30].

Model: A LNSM can be realized from the following tight-binding Hamiltonian on a cubic lattice

$$H = t_1 \sum_{\mathbf{k}} \Psi_{\mathbf{k}}^\dagger [\cos(k_x a) + \cos(k_y a) - b] \tau_1 \Psi_{\mathbf{k}} + \sum_{\mathbf{k}} \Psi_{\mathbf{k}}^\dagger [t_2 (\cos(k_z a) - 1) \tau_1 + t_3 \sin(k_z a) \tau_2] \Psi_{\mathbf{k}} \quad (1)$$

where a is the lattice spacing. The two-component spinor is defined as $\Psi_{\mathbf{k}}^\top = (c_{A,\mathbf{k}}, c_{B,\mathbf{k}})$. Here, $c_{j,\mathbf{k}}$ is the fermion annihilation operator on sublattice $j = A, B$ with momentum \mathbf{k} , and τ_1 and τ_2 are two off-diagonal Pauli matrices. The Hamiltonian is invariant under the reversal of time, generated by $\mathcal{T} = K$ where K is the complex conjugation and $\mathcal{T}^2 = +1$. The anticommutation relation $\{H, \tau_3\} = 0$ ensures the spectral symmetry of the system. The inversion symmetry (\mathcal{P}), under which $\mathbf{k} \rightarrow -\mathbf{k}$ and $\Psi_{\mathbf{k}} \rightarrow \tau_1 \Psi_{-\mathbf{k}}$ guarantees that an isolated nodal ring is pinned at the $k_z = 0$ plane. This LNSM supports topologically protected flat surface state at zero energy (image of the bulk loop), which is an eigenstate of τ_3 with eigenvalue ± 1 . Therefore, the drumhead shaped surface states are localized on *complimentary* sublattices on *opposite* surfaces along the (001) direction, see Fig. 1(b).

With the restoration of spin degrees of freedom and upon linearizing the above model near $\mathbf{k} = (0, 0, 0)$ point, we arrive at the continuum description of the LNSM

$$\hat{H}_0 = \Gamma_1 \left(\frac{k_\perp^2 - k_F^2}{2m} \right) + \Gamma_2 (v_z k_z) \equiv \sum_{j=1,2} \Gamma_j d_j, \quad (2)$$

where $m^{-1} = t_1 a^2$, $v_z = t_3 a$, $k_\perp^2 = k_x^2 + k_y^2$ and $k_F = \sqrt{2(2-b)}a^{-1}$, and $\Gamma_j = \sigma_0 \otimes \tau_j$. Pauli matrices σ_μ operate on the spin index. The radius of the nodal ring is k_F , around which $(k_\perp^2 - k_F^2)/(2m) \approx v_r k_r$, where $v_r = k_F/m$ is the radial Fermi velocity. Thus fermionic dispersion scales *linearly* with the radial ($k_r = k_\perp - k_F$) and \hat{z} components of momentum, and a LNSM corresponds to a $z = 1$ fixed point, where z is the *dynamic scaling exponent*. Besides \mathcal{P} and $\mathcal{T} (= i\sigma_2 \otimes \tau_0 K)$ symmetries, \hat{H}_0 is also invariant under $SU(2)$ chiral rotation of the spin quantization axis, generated by $\sigma \otimes \tau_0$.

Spontaneous symmetry breaking: Due to vanishing DOS [29], a LNSM remains stable against sufficiently weak, but generic short-range, such as onsite Hubbard (U), nearest-neighbor (V) interactions. However, strong repulsive interactions can destroy the noninteracting $z = 1$ fixed point and give rise to various BSPs. All together a LNSM can be susceptible to *seven* types of *intra-unit cell* instabilities in the particle-hole channels. The corresponding effective single particle Hamiltonian reads as $H_{SP} = \Delta_{\mu\nu} (\sigma_\mu \otimes \tau_\nu)$, where $\mu, \nu = 0, 1, 2, 3$ (except for $\mu = \nu = 0$, since Δ_{00} corresponds to chemical potential) and $\Delta_{\mu\nu} = \langle \Psi^\dagger \sigma_\mu \otimes \tau_\nu \Psi \rangle$ is the order parameter (OP). Physical meaning of various OPs and their transformation under symmetry operations are displayed in Table. I,

OP	Physical order	\mathcal{T}	\mathcal{P}	$SU(2)$	Susceptibility
Δ_{01}	Bond density	✓	✓	✓	$f(v_r, v_z)\Lambda/2$
Δ_{02}	Current density	×	×	✓	$f(v_r, v_z)\Lambda/2$
Δ_{03}	Charge density wave	✓	×	✓	$f(v_r, v_z)\Lambda$
Δ_{j0}	Ferromagnet	×	✓	×	0
Δ_{j1}	Spin bond density	×	✓	×	$f(v_r, v_z)\Lambda/2$
Δ_{j2}	Spin current density	✓	×	×	$f(v_r, v_z)\Lambda/2$
Δ_{j3}	Antiferromagnet	×	×	×	$f(v_r, v_z)\Lambda$

TABLE I: Various OPs, their physical realizations and transformations under various symmetry operations. Here ✓ and × stand for even and odd under a symmetry operation, respectively. The last column displays mean-field susceptibility of various orderings, where Λ is the ultraviolet cutoff and $f(v_r, v_z)$ is a nonuniversal, but positive definite function [31].

and due to the spin rotational symmetry, $\Delta_{j\nu} = |\vec{\Delta}_\nu|$ for $j = 1, 2, 3$ and any ν .

In the presence of underlying bond (Δ_{01}) and spin bond (Δ_{j1}) density orders, the nearest-neighbor hopping amplitude respectively acquires spin independent or dependent modulation, and the ordered phases support two nodal rings in the xy plane, with radii $k_\perp^\pm = [k_F^2 \pm 2m\Delta]^{1/2}$, for $\Delta = \Delta_{01}$ or $|\vec{\Delta}_1|$. By contrast, nucleation of Δ_{02} and Δ_{j2} respectively gives rise to current density and spin current density. These two ordered phases are also accompanied by two nodal rings, but they are of identical radius $k_\perp = k_F$, symmetrically placed about the xy plane at $k_z = \pm\Delta/v_z$ for $\Delta = \Delta_{j2}$ or $|\vec{\Delta}_2|$. On the other hand, the CDW (Δ_3) and AF ($|\vec{\Delta}_3|$) orders, respectively gives rise to staggered pattern of charge and spin, and concomitantly to a *fully gapped spectrum*. Onset of a ferromagnet ordering leads to the formation of compensated electron and hole doped line nodes for opposite spin projections[32], and thus lead to a subsequent BCS-like excitonic instability toward the formation of the AF order. But, the AF OP gets locked into the spin easy-plane, perpendicular to the ferromagnetic moment, and represents *canted antiferromagnet*.

Valuable insight into the propensity toward various orderings can be gained from their mean-field susceptibilities (χ) (see Table I). Note that the critical strength of interaction for any ordering is *inversely* proportional to χ . The CDW and AF orders possess the largest susceptibility, and consequently require minimal critical strengths of interaction for nucleation. Since at $T = 0$ optimal minimization of the free energy (no competition with entropy) naturally prefers fully gapped phases, generic and strong short-range interaction supports either CDW or AF orders over gapless phases. Despite being accompanied by *two* massless Goldstone mode (due to spontaneous breaking of spin rotational symmetry), the AF phase in a three dimensional LNSM can exhibit a genuine finite temperature continuous phase transition, described

by a three-component ϕ^4 theory, while that for the CDW phase is captured by a single-component ϕ^4 theory.

Proximity effect: While the nodal orderings give rise to drumhead shaped surface states on (001) surface in the ordered phases (images of the bulk nodal rings), onset of any mass ordering (such as CDW, AF) splits the surface states and place them at finite energies, as shown in Fig. 1(b). Since surface states, arising from the model shown Eq. (1), are completely flat, they can undergo various weak coupling instabilities [such as surface CDW when $V > U$ and AF when $U > V$ as shown in Fig. 1(b)] due to *diverging* DOS, before the bulk acquires propensity toward ordering. Such surface ordering in turn can reduce the critical strength for ordering in the bulk and induce corresponding BSP at weaker couplings. As the number of bulk states is much larger than that localized on the surface, in order to observe such proximity induced BSPs in the bulk one needs to systematically reduce the thickness of the system [30]. Therefore, the thickness of a LNSM may play the role of an experimentally accessible *nonthermal* tuning parameter to drive the system through a QPT and place it in a BSP. But, further quantitative estimation of such proximity induced ordering from the surface to bulk necessarily demands numerical analysis. Finally, it is also worth noticing that when $U > V$, each surface along (001) direction becomes *ferromagnet*, due to sublattice polarization of surface states, see Fig. 1(b). The magnetic moment, however, points in opposite direction on opposite surfaces, and the ordered phase represents a *layer or global antiferromagnet*. Next we investigate the onset of CDW and AF orders and their competition inside the bulk of a LNSM.

Phase diagram: The stability of a LNSM (for weak interactions), the possible onset of CDW, AF phases, and the competition between these two ordered phases (for strong interactions) can be demonstrated from the following mean field free energy density

$$F = \frac{\Delta_3^2}{2g_C} + \frac{|\vec{\Delta}_3|^2}{2g_{AF}} - 2 \sum_{\sigma=\pm} \int' \frac{d^3\mathbf{k}}{(2\pi)^3} E_\sigma(\mathbf{k}), \quad (3)$$

where $E_\sigma(\mathbf{k}) = \left[d_1^2 + d_2^2 + \Delta_3^2 + |\vec{\Delta}_3|^2 + 2\sigma\Delta_3|\vec{\Delta}_3| \right]^{1/2}$. The integral over momentum is restricted up to an ultraviolet cutoff Λ . In the presence of onsite (U) and nearest-neighbor (V) repulsions (extended Hubbard model), the interacting Hamiltonian reads as

$$H_I = U \sum_{\vec{x}} n_{\uparrow}(\vec{x})n_{\downarrow}(\vec{x}) + \frac{V}{2} \sum_{\vec{a},j,\sigma,\sigma'} n_{\sigma}(\vec{a})n_{\sigma'}(\vec{a} + \vec{b}_j) \quad (4)$$

and we obtain $g_C = (6V - U)/8$ and $g_{AF} = U/8$. Here, $n_{\sigma}(\vec{x})$ is the fermionic number at \vec{x} , with spin projection $\sigma = \uparrow, \downarrow$ and sites on A (B) sublattice are located at \vec{a} ($\vec{a} + \vec{b}_j$ where $j = 1, \dots, 6$).

Let us first focus on a simpler situation with only CDW order, i.e., when $|\vec{\Delta}_3| = 0$. Minimizing F we then obtain

the following gap equation

$$g_C \int_0^{E_\Lambda} d\varepsilon \frac{\varrho(\varepsilon)}{\sqrt{\varepsilon^2 + \Delta_3^2}} = 1, \quad (5)$$

where E_Λ is the ultraviolet energy up to which the quasi-particle dispersion in a LNSM is linear. The above gap equation yields nontrivial solution for order parameters

$$\delta_C = 1 + m_C - \sqrt{1 + m_C^2} \quad (6)$$

where $m_C = \Delta_3/E_\Lambda$ is the dimensionless CDW OP, $\delta_C = [(g_C^*)^{-1} - g_C^{-1}] E_\Lambda^{-1}$, only when interaction is stronger than a critical one (g_C^*), i.e. $g_C > g_C^*$. In close proximity to the quantum critical point (QCP), located at $g_C = g_C^*$, $m_C \ll 1$, yielding $m_C \sim \delta_C$. Therefore, general scaling relation $m_C \sim \delta_C^{\nu z}$, suggests that $\nu z = 1$, where ν is the *correlation length exponent*. A similar self-consistent solution can be found for the AF order upon setting $\Delta_3 = 0$ in Eq. (3). Hence, CDW and AF orderings set in beyond a critical strength of interaction through a continuous QPT and the transition temperature for these two ordering scales as $T_c \sim |\delta|^{\nu z}$. By solving the coupled gap equations and simultaneously minimizing the free energy [31], we arrive at the phase diagram of an interacting LNSM, shown in Fig. 1(a). The transition between AF and CDW orders is, however, *first order* in nature.

Similar phase diagram can be obtained from a renormalization group analysis, controlled via a simultaneous large N_f , where N_f is the number of fermionic component and ϵ expansions, where $\epsilon = d_c - 1$, about the lower critical co-dimension $d_c = 1$ (representing a Fermi surface) [29, 31, 33]. For a three dimensional LNSM $d_c = 2$, and scaling dimension of local four fermion interaction $[g_j] = -\epsilon$, confirming that sufficiently weak interaction is an irrelevant perturbation. As $N_f \rightarrow \infty$, we find $\nu = \epsilon^{-1}$ and $z = 1$ at all QCPs. For $\epsilon = 1$, thus $\nu = 1$ at all QCPs (far from the mean-field value $\nu = 1/2$), which, however, is only an artifact fact of $N_f \rightarrow \infty$ approximation and expected to be different at various QCPs once $1/N_f$ corrections are taken into account.

Long range interaction: As a penultimate topic we comment on the effect of long range tail of the Coulomb interaction on various ordering. Leading corrections to the *anomalous dimension* of various fermion bilinears or OPs due to Coulomb interaction is largest for *mass* orders (CDW and AF) and proportional to $\alpha_r F(\eta)/\Lambda$, where $\alpha_r = e^2/(4\pi^2 v_r)$ is the fine structure constant in the radial direction, $\eta = v_z/v_r$, $F(\eta) = E_k(1 - \eta^2) + E_k(1 - \eta^{-2})/\eta$ and E_k is the elliptic function of first kind [31]. Thus long range Coulomb interaction can enhance the propensity toward mass ordering in LNSM, at least when weak. A complete analysis on the interplay of long range and short range Coulomb interactions is an involved task and deserves a separate investigation.

Superconductivity: Finally we shed light on possible paired states in a LNSM, when electronic interaction ac-

quires a strong attractive component. We now introduce a Nambu doubled spinor as $\Psi_N = (\Psi_p, \Psi_h)^\top$, where $\Psi_p = (\Psi_{p,\uparrow}, \Psi_{p,\downarrow})^\top$, $\Psi_h = (\Psi_{h,\downarrow}, -\Psi_{h,\uparrow})^\top$ and $\Psi_{p,s}^\top = (\Psi_{A,s}^\dagger, \Psi_{B,s}^\dagger)$, $\Psi_{h,s}^\top = (\Psi_{B,s}, \Psi_{A,s})$ for $s = \uparrow / \downarrow$ [34]. In this basis $\vec{S} = \eta_0 \otimes \vec{\sigma} \otimes \tau_0$ are the three generators of electron spin and the non-interacting Hamiltonian becomes $\hat{H}_0^N = \eta_3 \otimes \Gamma_1 d_1 + \eta_0 \otimes \Gamma_2 d_2$, where the Pauli matrices η_μ operate on the Nambu index. All together the LNSM permits *four* local pairings, and the corresponding effective single-particle Hamiltonian reads as $H_{SC} = (\eta_1 \cos \phi + \eta_2 \sin \phi) \otimes H_p$, where ϕ is the superconducting phase and

$$H_p = \Delta_s \Gamma_1 + \Delta_0 \Gamma_0 + \Delta_2 \Gamma_2 + \Delta_t \vec{\sigma} \otimes \tau_3. \quad (7)$$

First three pairings are spin-singlet, while the last one is spin-triplet, among which only the spin singlet s -wave pairing (Δ_s) stands as *Majorana mass* [1]. Remaining three pairings support gapless BdG quasiparticle around nodal rings inside the ordered phase, and thus expected to be energetically inferior to the fully gapped s -wave pairing [31]. It should be noted that due to the presence of flat surface states the s -wave pairing can take place on the surface in even for sufficiently weak attractive interaction, which can also be mediated by electron-phonon interaction. Such surface superconductivity can in turn induce pairing among the bulk states through proximity effect, in particular for a thin film of a LNSM.

Upon casting *six* matrices corresponding to the mass orders (AF, CDW, s -wave pairing) in Nambu representation, we can arrange them into two sets according to

$$\{\eta_3 \otimes \vec{\sigma} \otimes \tau_3\} \text{ and } \{\eta_0 \otimes \sigma_0 \otimes \tau_3, \vec{\eta}_\perp \otimes \sigma_0 \otimes \tau_1\}.$$

Together they constitute a $Cl(3) \times Cl(3)$ algebra, where $\vec{\eta}_\perp = (\eta_1, \eta_2)$ [35]. Therefore, both strong onsite Hubbard repulsion and attraction can destabilize a LNSM, by respectively supporting an AF order or through simultaneous nucleation of a CDW and s -wave superconductor, both of which spontaneously break a genuine $SU(2)$ symmetry. These two transitions thus belong to the same universality class, which can be demonstrated in numerical simulation. Such exact symmetry between CDW and s -wave pairing stems from the bipartite nature of the cubic lattice and absence of particle-hole asymmetry in the normal state and any other finite range component of Coulomb interaction. For example, weak repulsive (attractive) nearest-neighbor interaction lifts such degeneracy and prefers CDW (s -wave pairing).

Conclusions: To conclude, we here show that LNSM can be a fertile ground to observe a plethora of BSPs in the bulk (for strong interaction) as well as on the surface (for weak interaction). The weak coupling instabilities of drumhead shaped flat surface states can in turn induce orderings in the bulk through proximity effect even for weaker interaction, making our proposals relevant in

real materials [11–28]. By contrast, if a LNSM lacks \mathcal{T} symmetry or spin degeneracy [26], coined as Weyl-loop semimetal, the number of possible ordering channels is quite reduced, with *ferromagnet* standing as the only possible mass order [31]. Nevertheless, our conclusions regarding the fate of the QPT and surface induced proximity effect into bulk remains unchanged in this system.

Acknowledgments: This work was supported by ARO-Atomtronics-MURI, NSF-JQI-PFC and LPS-MPO-CMTC. The author is grateful to Victor Galitski for continued interest in this work and many stimulating discussions. B. R. also thanks C-K. Chiu, I. Herbut for discussions, P. Goswami, V. Juričić for critical reading of the manuscript, and Nordita, Center for Quantum Materials for hospitality.

-
- [1] Any ordering that fully gaps out quasiparticle excitation is referred as *mass*. When such ordering occurs in the pairing channel, we coin it as *Majorana mass*.
 - [2] R. Dornhaus, G. Nimitz, and B. Schlicht, *Narrow-Gap Semicconductors*, (Springer-Verlag, 1983).
 - [3] Y.-H. Chan, C-K. Chiu, M. Y. Chou, A. P. Schnyder, arXiv:1510.02759
 - [4] T. Bzdušek, Q. S. Wu, A. Rüegg, M. Sigrist, A. A. Soluyanov, arXiv:1604.03112
 - [5] Y. Huh, E-G. Moon, Y. B. Kim, Phys. Rev. B **93**, 035138 (2016).
 - [6] J-W. Rhim, Y. B. Kim, New J. Phys. **18**, 043010 (2016)
 - [7] Z. Yan, P-W. Huang, Z. Wang, Phys. Rev. B **93**, 085138 (2016)
 - [8] P. Goswami, and A. H. Nevidomskyy, Phys. Rev. B **92**, 214504 (2015).
 - [9] R. Nandkishore, Phys. Rev. B **93**, 020506 (2016).
 - [10] S. E. Han, G. Y. Cho, E-G. Moon, arXiv:1601.00975
 - [11] M. N. Ali, Q. D. Gibson, T. Klimczuk, and R. J. Cava, Phys. Rev. B **89**, 020505(R) (2014).
 - [12] L. S. Xie, L. M. Schoop, E. M. Seibel, Q. D. Gibson, W. Xie and R. J. Cava, APL Mat. **3** 083602 (2015).
 - [13] G. Bian, T.-R. Chang, R. Sankar, S.-Y. Xu, H. Zheng, T. Neupert, C.-K. Chiu, S.-M. Huang, G. Chang, I. Belopolski, D. S. Sanchez, M. Neupane, N. Alidoust, C. Liu, B. Wang, H.-T. Jeng, A. Bansil, F. Chou, H. Lin, and M. Z. Hasan, Nature Commun. **7**, 10556 (2016).
 - [14] G. Bian, T-R. Chang, H. Zheng, S. Velury, S-Y. Xu, T. Neupert, C-K. Chiu, D. S. Sanchez, I. Belopolski, N. Alidoust, P-J. Chen, G. Chang, A. Bansil, H-T. Jeng, H. Lin, M. Z. Hasan, Phys. Rev. B **93**, 121113 (2016).
 - [15] A. A. Burkov, M. D. Hook, L. Balents, Phys. Rev. B **84**, 235126 (2011).
 - [16] E. K-H. Lee, S. Bhattacharjee, K. Hwang, H.-S. Kim, H. Jin, Y. B. Kim, Phys. Rev. B **89**, 205132 (2014).
 - [17] M. Phillips, V. Aji, Phys. Rev. B **90**, 115111 (2014).
 - [18] Y. Chen, Y. Xie, S. A. Yang, H. Pan, F. Zhang, M. L. Cohen, and S. Zhang, Nano Lett. **15**, 6974 (2015).
 - [19] H. Weng, Y. Liang, Q. Xu, R. Yu, Z. Fang, X. Dai, and Y. Kawazoe, Phys. Rev. B **92**, 045108 (2015).
 - [20] Y. Kim, B. J. Wieder, C.?L. Kane, and A. M. Rappe, Phys. Rev. Lett. **115** 036806 (2015).

- [21] R. Yu, H. Weng, Z. Fang, X. Dai, and X. Hu, Phys. Rev. Lett. **115**, 036807 (2015).
- [22] M. Zeng, C. Fang, G. Chang, Y-A. Chen, T. Hsieh, A. Bansil, H. Lin, L. Fu, arXiv:1504.03492
- [23] J. Zhao, R. Yu, H. Weng, Z. Fang, arXiv:1511.05704
- [24] A. Yamakage, Y. Yamakawa, Y. Tanaka, and Y. Okamoto, J. Phys. Soc. Jpn. **85**, 013708 (2016).
- [25] M. Hirayama, R. Okugawa, T. Miyake, S. Murakami, arXiv:1602.06501
- [26] P. Goswami, B. Roy, and S. Das Sarma, arXiv:1603.02273
- [27] H. Huang, J. Liu, D. Vanderbilt, W. Duan, arXiv:1605.04050
- [28] D. Takane, Z. Wang, S. Souma, K. Nakayama, C. X. Trang, T. Sato, T. Takahashi, Yoichi Ando, arXiv:1606.07957
- [29] DOS scales as $\rho(\varepsilon) \sim |\varepsilon|^{-1+d_c/z}$, where d_c is the co-dimension, equals to the difference between the physical dimension and dimensionality of the hyperplane over which energy gap vanishes. The co-dimension of a LNSM (Fermi surface) is $d_c = 2(1)$, yielding linearly vanishing (constant) DOS, since $z = 1$ for linearly dispersing quasiparticles around Fermi energy.
- [30] The finite size effect or hybridization induced gap for the surface states ($\sim 1/L$) is assumed to be $\ll U$ or V .
- [31] See Supplementary Materials for details of calculation.
- [32] Ferromagnetism can arise from Zeeman coupling when the system is placed in magnetic field.
- [33] T. Senthil, and R. Shankar, Phys. Rev. Lett. **102**, 046406 (2009).
- [34] B. Roy, Phys. Rev. B **88**, 075415(2013).
- [35] $Cl(3)$ defines a set of three mutually anticommuting matrices.

Supplementary Materials for “*Interacting line-node semimetal and spontaneous symmetry breaking*”

Bitan Roy¹

¹*Condensed Matter Theory Center and Joint Quantum Institute, University of Maryland, College Park, Maryland 20742-4111, USA*

The Supplementary Material contains:

1. Minimal representation and no-doubling theorem for three dimensional line-node semimetals,
2. Mean field susceptibility of various orders in a line-node semimetal,
3. Mean field gap equation in the presence of charge-density-wave and antiferromagnet orders,
4. Large N renormalization group analysis, capturing transition into various broken symmetry phases,
5. Correction to anomalous dimensions for various fermion bilinears due to long range Coulomb interaction,
6. Derivation of $Cl(3) \times Cl(3)$ algebra among mass matrices in a line-node semimetal from Clifford algebra,
7. Quasi-particle spectrum inside various superconducting ground states and their symmetries.

• **Minimal representation of a three dimensional line node semimetal:** We first demonstrate the minimal representation for a Dirac-loop and Weyl-loop semimetals. Recall that the tight-binding Hamiltonian for any line-node semimetal in a cubic lattice reads as

$$H = t_1 \sum_{\mathbf{k}} \Psi_{\mathbf{k}}^\dagger [\cos(k_x a) + \cos(k_y a) - b] \tau_1 \Psi_{\mathbf{k}} + \sum_{\mathbf{k}} \Psi_{\mathbf{k}}^\dagger [t_2 (\cos(k_z a) - 1) \tau_1 + t_3 \sin(k_z a) \tau_2] \Psi_{\mathbf{k}}, \quad (8)$$

where a is the lattice spacing, as announced in the main part of the paper. For now we do not specify the dimensionality of spinor basis. Two mutually anticommuting matrices τ_1 and τ_2 , satisfying the relation $\{\tau_1, \tau_2\} = 0$. The above model supports sharp gapless quasiparticle excitation around an isolated ring in the $k_z = 0$ plane when $|b| < 2$, and the term proportional to t_2 plays the role of momentum dependent Wilson mass. Without any loss of generality we choose $\tau_1(\tau_2)$ to be purely real (imaginary).

Let us first focus on a line-node semimetal that remains invariant under the reversal of time. The time-reversal operator $\mathcal{T} = UK$, where U is unitary operator and K is complex conjugation. Thus time-reversal symmetry of the Hamiltonian operator mandates that $\mathcal{T} = K$, with $\mathcal{T}^2 = +1$. Hence, one can realize a isolated nodal ring in the momentum space, arising from hopping of spinless fermions among the nearest-neighbor sites of two interpenetrating sublattices of a cubic lattice [1], and we can define the spinor basis as $\Psi_{\mathbf{k}}^\dagger = (c_{A,\mathbf{k}}, c_{B,\mathbf{k}})$. Here, $c_{j,\mathbf{k}}$ is the fermion annihilation operator on sublattice $j = A, B$ with momentum \mathbf{k} . Two anticommuting matrices τ_1 and τ_2 can, therefore, be chosen as standard off-diagonal Pauli matrices. Therefore, a Dirac-loop semimetal (DLSM) is devoid of doubling of the number of loops in the momentum space while preserving the \mathcal{T} symmetry, and a two component DLSM can be realized for spinless fermion from a microscopic tight-binding model. This situation is quite different than the one for two and three dimensional Dirac-node semimetals, for which the minimal representation for Dirac

spinor (without the standard doubling due to real spin of fermion) is respectively four and eight [2–4].

For a time-reversal symmetry breaking Weyl-loop semimetal we can choose $\mathcal{T} = i\tau_2 K$ and the Hamiltonian does not preserve the \mathcal{T} symmetry. Hence, $\mathcal{T}^2 = -1$, and we can define a two component spinor as $\Psi_{\mathbf{k}}^T = (c_{\uparrow, \mathbf{k}}, c_{\downarrow, \mathbf{k}})$, where $s = \uparrow / \downarrow$ are two projections of spin. Thus an isolated Weyl-loop can be realized in a \mathcal{T} breaking system from spin dependent hopping on a cubic lattice. Two Kramers non-degenerate bands (valence and conduction) touch at each point of such ring in the Brillouin zone. The system is named as Weyl-loop semimetal (WLSM). Therefore, WLSM as well does not suffer from fermion doubling unlike three dimensional Weyl-node semimetal.

The absence of the third Pauli matrix τ_3 ensures the spectral symmetry of H , while the inversion symmetry (\mathcal{P}), under which $\mathbf{k} \rightarrow -\mathbf{k}$ and $\Psi_{\mathbf{k}} \rightarrow \tau_1 \Psi_{-\mathbf{k}}$ guarantees that the nodal ring is pinned at the $k_z = 0$ plane.

• **Susceptibility of various orders:** We now display evaluation of susceptibility for various fermionic bilinears or order parameters (OPs) in a DLMS. For a given OP $\Delta_{\mu\nu} = \langle \Psi^\dagger \sigma_\mu \otimes \tau_\nu \Psi \rangle$, the mean field susceptibility (for zero external frequency and momentum) is given by

$$\chi_{\mu\nu} = -2 \mathbf{Tr} \int' \frac{dk_r dk_z}{(2\pi)^2} \int_{-\infty}^{\infty} \frac{d\omega}{2\pi} \left[(\sigma_\mu \otimes \tau_\nu) \frac{i\omega + \hat{H}_0}{\omega^2 + v_r^2 k_r^2 + v_z^2 k_z^2} (\sigma_\mu \otimes \tau_\nu) \frac{i\omega + \hat{H}_0}{\omega^2 + v_r^2 k_r^2 + v_z^2 k_z^2} \right], \quad (9)$$

where $\hat{H}_0 = \sigma_0 \otimes (\tau_1 v_r k_r + \tau_2 v_z k_z)$. Here ω is the fermionic Matsubara frequency and \mathbf{Tr} is operative over four dimensional matrices. For various choices of μ and ν (accept for $\mu = \nu = 0$ for which Δ_{00} represents the chemical potential), we find

$$\begin{aligned} \chi_{03} = \chi_{j3} &= \frac{N_f}{\pi^2} \int' \frac{dk_r dk_z}{(2\pi)^2} \frac{1}{\sqrt{v_r^2 k_r^2 + v_z^2 k_z^2}}, & \chi_{01} = \chi_{j1} &= \frac{N_f}{2\pi^2} \int' \frac{dk_r dk_z}{(2\pi)^2} \left[\frac{1}{\sqrt{v_r^2 k_r^2 + v_z^2 k_z^2}} + \frac{v_r^2 k_r^2 - v_z^2 k_z^2}{[v_r^2 k_r^2 + v_z^2 k_z^2]^{3/2}} \right], \\ \chi_{02} = \chi_{j2} &= \frac{N_f}{2\pi^2} \int' \frac{dk_r dk_z}{(2\pi)^2} \left[\frac{1}{\sqrt{v_r^2 k_r^2 + v_z^2 k_z^2}} + \frac{-v_r^2 k_r^2 + v_z^2 k_z^2}{[v_r^2 k_r^2 + v_z^2 k_z^2]^{3/2}} \right], \\ \chi_{j0} = 8N_f \int' \frac{dk_r dk_z}{(2\pi)^2} \int_{-\infty}^{\infty} \frac{d\omega}{2\pi} \frac{\omega^2 - (v_r^2 k_r^2 + v_z^2 k_z^2)}{(\omega^2 + v_r^2 k_r^2 + v_z^2 k_z^2)^2} &= 0, \end{aligned} \quad (10)$$

after completing the integral over Matsubara frequency ω , for $j = 1, 2, 3$. Here N_f represents the number of four component spinor. The integral over spatial components of momentum is restricted within $0 < k_r < \Lambda$ and $0 < |k_z| < \Lambda$. Thus momentum integral can easily be performed by introducing a new set of variable as $v_r k_r = vk \sin \theta$ and $v_z k_z = vk \cos \theta$, and the integrals over newly introduced variables are restricted within the region $0 < k < \Lambda$ and $0 \leq \theta \leq \pi$. Finally we obtain

$$\chi_{03} = \chi_{j3} = \left[\frac{vN_f}{\pi v_r v_z} \right] \Lambda, \quad \chi_{01} = \chi_{02} = \chi_{j1} = \chi_{j2} = \left[\frac{vN_f}{\pi v_r v_z} \right] \frac{\Lambda}{2}, \quad \chi_{j0} = 0. \quad (11)$$

We have quoted this result in the main part of the paper, with $f(v_r, v_z) = (vN_f)/(\pi v_r v_z)$. The critical couplign for any such ordering $g_c^{\mu\nu} \propto \chi_{\mu\nu}^{-1}$.

• **Mean-field gap equation:** We here demonstrate the derivation and solution of the mean field gap equation, announced in the main part of the paper, in the presence of charge-density-wave (CDW) and antiferromagnet (AF) orderings. For concreteness, we also display the calculation for the self-consistent solution for the CDW order parameter (Δ_3). Similar calculation can also be carried out for the AF order parameter ($|\vec{\Delta}_3|$). The energy spectrum in the presence of these two order parameters (OPs) reads as

$$E_{\mathbf{k}, \sigma} \left(\Delta_3, |\vec{\Delta}_3| \right) = \pm \sqrt{\left(\frac{k_{\perp}^2 - k_F^2}{2m} \right)^2 + v_z^2 k_z^2 + \Delta_3^2 + |\vec{\Delta}_3|^2 + 2\sigma \Delta_3 |\vec{\Delta}_3|}, \quad (12)$$

for $\sigma = \pm$. The corresponding free energy in the presence of these two orderings is

$$F \left(\Delta_3, |\vec{\Delta}_3| \right) = \frac{\Delta_3^2}{2g_C} + \frac{|\vec{\Delta}_3|^2}{2g_{AF}} - 2 \sum_{\sigma=\pm} \int' \frac{d^3 \mathbf{k}}{(2\pi)^3} E_{\mathbf{k}, \sigma} \left(\Delta_3, |\vec{\Delta}_3| \right), \quad (13)$$

where $g_C = (6V - U)/8$ and $g_{AF} = U/8$ are the local four fermion interaction that respectively supports the CDW and AF orders. Here, U and V are the strength of onsite and nearest-neighbor repulsions.

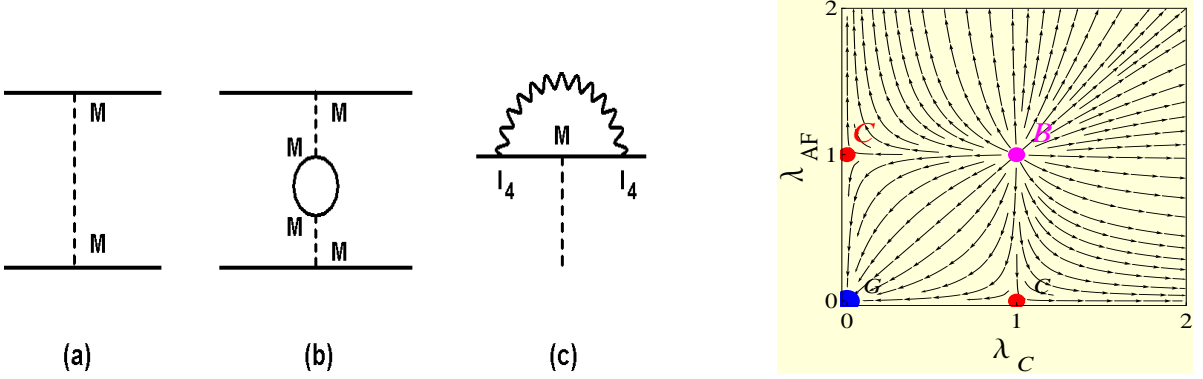


FIG. 2: Left: Feynman diagram (a) represents a bare four-fermion interaction coupling (g). Diagram (b) is the only relevant one-loop diagram, giving rise to renormalization of bare interaction vertex, in the large N_f limit. Here M is a four component Hermitian matrix, and solid lines represents fermions. (c) Leading order correction to the anomalous dimension of a fermion bilinear $\Psi^\dagger M \Psi$ due to the long range tail of the Coulomb interaction (represented by the wavy line). Here I_4 is the four dimensional identity matrix. Right: RG flow diagram in $(\lambda_C, \lambda_{AF})$ plane for $\epsilon = 1$. Here, the blue dot represents fully stable Gaussian fixed point representing a DLSP, while the red dots stand for quantum critical points. These two quantum critical points controls the continuous transition from a DLSP to CDW (one residing on $\lambda_{AF} = 0$ axis) and AF (one residing on $\lambda_C = 0$ axis) phases. The magenta dot is the bicritical point, controlling the first order transition between AF and CDW phases.

Let us first focus on the CDW ordering separately, and set $|\vec{\Delta}_3| = 0$. Then minimizing the free energy we arrive at the following mean field gap equation (after taking $2g_C \rightarrow g_C$)

$$\frac{1}{g_C} = \int \frac{d^3\mathbf{k}}{(2\pi)^3} \frac{1}{E_{\mathbf{k}}(\Delta_3)} \Rightarrow \frac{1}{g_C} = \int_0^{E_\Lambda} d\varepsilon \frac{\varrho(\varepsilon)}{\sqrt{\varepsilon^2 + \Delta_3^2}} \Rightarrow \frac{1}{g_C} - \int_0^{E_\Lambda} d\varepsilon = \int_0^{E_\Lambda} d\varepsilon \left[\frac{\varrho(\varepsilon)}{\sqrt{\varepsilon^2 + \Delta_3^2}} - 1 \right], \quad (14)$$

where $\varrho(\varepsilon) \sim |\varepsilon|$ is the density of states in a line-node semimetal and E_Λ is the high energy cutoff up to which the dispersion is linear. In term of a dimensionless parameter δ_C , defined as $\delta_C = [1/g_C^* - 1/g_C] E_\Lambda^{-1}$ the solution of the above gap equation is

$$\delta_C = 1 + m_C - \sqrt{1 + m_C^2}, \quad (15)$$

where $m_C = \Delta_3/E_\Lambda$ is the dimensionless CDW OP, as shown in the main part of the paper. The parameter δ_C measures the distance from the nonuniversal strength of critical nearest-neighbor interaction (g_C^*) for the CDW ordering. Similar self consistent solution can also be found for the AF OP in the absence of CDW OP, i.e. when $\Delta_3 = 0$.

The coupled gap equations in the presence of these two orderings read as

$$\frac{1}{g_C} = 2 \sum_{\sigma=\pm} \int' \frac{d^3\mathbf{k}}{(2\pi)^3} \frac{[1 + 2\sigma\Delta_3|\vec{\Delta}_3|^{-1}]}{E_{\mathbf{k},\sigma}(\Delta_3, |\vec{\Delta}_3|)}, \quad \frac{1}{g_{AF}} = 2 \sum_{\sigma=\pm} \int' \frac{d^3\mathbf{k}}{(2\pi)^3} \frac{[1 + 2\sigma|\vec{\Delta}_3|\Delta_3^{-1}]}{E_{\mathbf{k},\sigma}(\Delta_3, |\vec{\Delta}_3|)}. \quad (16)$$

We numerically solve these two coupled gap equations in ‘‘Mathematica’’ and minimize the free energy to obtain the phase diagram, displayed as Fig. 1 (a) in the main part of the paper.

• **Large- N renormalization group calculation:** To anchor the nature of the QPTs from a DLSP to BSPs and between two distinct BSPs, we perform a renormalization group (RG) calculation. The Euclidean action for minimal interacting model reads as

$$S = \int \frac{d\omega}{2\pi} \int' d^{1+\epsilon}\mathbf{k} \int d\theta \Psi_\alpha^\dagger [-i\omega + H_0] \Psi_\alpha - \sum_{j=C,AF} g_j \int \prod_{i=1}^3 \frac{d\omega_i}{2\pi} \int' d^{1+\epsilon}\mathbf{k}_i \int d\theta_i \left(\Psi_{1+2-3}^\dagger M_j \Psi_1 \right) \left(\Psi_3^\dagger M_j \Psi_2 \right) \quad (17)$$

where $\alpha \equiv (\omega, \mathbf{k}, \theta)$, $H_0 = \Gamma_1 v_r k_r + \Gamma_2 v_z k_z$, $M_C = \sigma_0 \otimes \tau_3$ and $M_{AF} = \vec{\sigma} \otimes \tau_3$. Fermionic field Ψ_i ($i = 1, \dots, 4$) is a function of $\alpha_i \equiv (\omega_i, \mathbf{k}_i, \theta_i)$. The integral over momentum is restricted up to an ultraviolet cut-off Λ . The scaling dimension of four-fermion interaction is $[g_j] = 1 - d_c$, where d_c is the *co-dimension*. For a three dimensional DLSM is $d_c = 2$ [8, 9]. Hence $[g_j] = -1$ and sufficiently weak short-range interaction is an *irrelevant* perturbation in a DLSM and the potential breakdown of the noninteracting fixed point at strong interaction can be demonstrated via a RG calculation, controlled via a simultaneous $1/N_f$ and ϵ -expansions about a lower critical co-dimension $d_c^* = 1$ (representing a Fermi surface), where N_f is the number of four-component spinor and $\epsilon = d_c - 1$.

We now present some essential details of the renormalization group calculation performed using simultaneous large N_f and ϵ -expansion in a DLSM. In the $N_f \rightarrow \infty$ limit only diagram (b) from Fig. 2 contributes to the renormalization of the bare interaction coupling. The contribution from this diagram reads as

$$(1, b) = -2g_j^2 \mathbf{Tr} \int' \frac{dk_r dk_z}{(2\pi)^2} \int_{-\infty}^{\infty} \frac{d\omega}{2\pi} \left[M_j \frac{i\omega + \hat{H}_0}{\omega^2 + v_r^2 k_r^2 + v_z^2 k_z^2} M_j \frac{i\omega + \hat{H}_0}{\omega^2 + v_r^2 k_r^2 + v_z^2 k_z^2} \right], \quad (18)$$

where $M_j = \sigma_0 \otimes \tau_3$ and $\vec{\sigma} \otimes \tau_3$ respectively for $j = C, AF$. After completing the frequency integral we obtain

$$(1, b) = \frac{g_j^2 N_f}{\pi^2} \int' dk_r dk_z \frac{1}{\sqrt{v_r^2 k_r^2 + v_z^2 k_z^2}} = \frac{g_j^2 N_f \Lambda^\epsilon}{\pi v} = g_j \lambda_j, \quad (19)$$

after integrating over the Wilsonian shell $\Lambda e^{-l} < k_r < \Lambda$ and $\Lambda e^{-l} < |k_z| < \Lambda$, where $\lambda_j = \frac{g_j N_f \Lambda^\epsilon}{\pi v}$ is the dimensionless coupling constant. Upon performing subsequent rescale according to $\omega \rightarrow e^{-l} \omega$, $k_{r/z} \rightarrow e^{-l} k_{r/z}$, $\Psi \rightarrow e^{(3+\epsilon)l/2} \Psi$, we arrive at the flow equations

$$\frac{d\lambda_C}{dl} = -\epsilon \lambda_C + \lambda_C^2, \quad \frac{d\lambda_{AF}}{dl} = -\epsilon \lambda_{AF} + \lambda_{AF}^2, \quad (20)$$

in $N_f \rightarrow \infty$ limit.

All together, the above flow equations support four fixed point: (i) $(\lambda_C, \lambda_{AF}) = (0, 0)$, (ii) $(\lambda_C, \lambda_{AF}) = (\epsilon, 0)$, (iii) $(\lambda_C, \lambda_{AF}) = (0, \epsilon)$ and (iv) $(\lambda_C, \lambda_{AF}) = (\epsilon, \epsilon)$, as shown in Fig. 2 (Right) (after setting $\epsilon = 1$). The first one is a fully stable Gaussian fixed point, representing a stable DLSM for sufficiently weak interactions. The second and third ones are quantum critical points (QCPs) with only one unstable direction, respectively describing the transition to CDW and AF phases for sufficiently strong $\lambda_C \sim V$ and $\lambda_{AF} \sim U$. The last one is a bicritical point with two unstable directions, indicating a first order transition between these two distinct BSPs. The corresponding phase diagram in the $(V/U_c, U/U_c)$ plane is shown in Fig. 2 (Right), where U_c is the nonuniversal critical strengths of onsite repulsions for AF orderings. Similar scaling analysis and RG calculation indicates the onset of a \mathcal{P} , \mathcal{T} -odd magnetic ordering (Δ_M) through a continuous QPT for sufficiently strong Hubbard interaction in WLSM.

• **Correction to anomalous dimension of various fermion bilinears due to long range Coulomb interaction:** We now discuss the correction to the anomalous dimension of various fermion bilinears, represented as $\Psi^\dagger M \Psi$, where M is a four dimensional Hermitian matrix due to long range Coulomb interaction in a DLSM. Such correction to the anomalous dimension arises from diagram (c) in Fig. 2. Contribution from this diagram reads as

$$\chi_{\mu\nu}^C = -2e^2 \int' \frac{dk_r dk_z}{(2\pi)^2} \int_{-\infty}^{\infty} \frac{d\omega}{2\pi} \frac{i\omega + \hat{H}_0}{\omega^2 + v_r^2 k_r^2 + v_z^2 k_z^2} (\sigma_\mu \otimes \tau_\nu) \frac{i\omega + \hat{H}_0}{\omega^2 + v_r^2 k_r^2 + v_z^2 k_z^2} \frac{1}{k_r^2 + k_z^2}, \quad (21)$$

where e is the electronic charge. Upon completing the integral over the Matsubara frequency we find

$$\begin{aligned} \chi_{03}^C &= \chi_{j3}^C = \frac{e^2}{4\pi^2 v_r} \int' \frac{dk_r dk_z}{(k_r^2 + \eta^2 k_z^2)^{1/2}} \frac{1}{k_r^2 + k_z^2}, & \chi_{0j}^C &= 0, \\ \chi_{01}^C &= \chi_{02}^C = \chi_{j1}^C = \chi_{j2}^C = \frac{e^2}{8\pi^2 v_r} \int' \frac{dk_r dk_z}{(k_r^2 + \eta^2 k_z^2)^{1/2}} \frac{1}{k_r^2 + k_z^2}, \end{aligned} \quad (22)$$

where $\eta = v_z/v_r$. Next we integrate out a thin Wilsonian shell with $\Lambda e^{-l} < q_r < \Lambda$ and $\Lambda e^{-l} < |q_z| < \Lambda$, to capture the enhancement of anomalous dimension. We find

$$\chi_{03}^C = \chi_{j3}^C = \frac{\alpha_r}{\Lambda} F(\eta) l \quad \text{and} \quad \chi_{01}^C = \chi_{02}^C = \chi_{j1}^C = \chi_{j2}^C = \frac{1}{2} \frac{\alpha_r}{\Lambda} F(\eta) l, \quad (23)$$

where $\alpha_r = e^2/(4\pi^2 v_r)$ can be considered as the fine structure constant along the radial direction. The function

$$F(\eta) = E_k(1 - \eta^2) + \frac{E_k(1 - \eta^{-2})}{\eta}, \quad (24)$$

where E_k is the elliptic function of first kind. Therefore, mass orderings receive largest boost through the enhancement of anomalous dimension due to the long range tail of the Coulomb interaction in a DLSM, as announced in the main part of the paper. Similar conclusion can readily be generalized for WLSM, suggesting that a ferromagnetic order receives largest boost in anomalous dimension from long range tail of the Coulomb interaction.

• **Derivation of internal algebra among masses in a Dirac-loop semimetal (DLSM):** We here provide a proof of $Cl(3) \times Cl(3)$ algebra among various mass matrices (representing two insulators and one superconductor) in a DLSM. Our derivation is based on Clifford algebra and does not rely on specific microscopic details of the model. Let us define a Nambu-doubled spinor as $\Psi = (\Psi_p, \Psi_h)^\top$ so that the effective Hamiltonian describing low energy excitations in a DLSM assumes the form

$$H_{DL}(\mathbf{k}) = H_0(\mathbf{k}) \oplus [-H_0^\top(-\mathbf{k})], \quad (25)$$

where

$$H_0(\mathbf{k}) = \sum_{j=1,2} \alpha_j d_j(\mathbf{k}), \quad \text{and} \quad d_1(\mathbf{k}) = \frac{k_x^2 + k_y^2 - k_F^2}{2m}, \quad d_2(\mathbf{k}) = v_z k_z. \quad (26)$$

Here α_1 and α_2 are two mutually anticommuting four component Hermitian matrices. Next we wish to find all the Hermitian eight dimensional matrices (M s) that anticommute with $H_{DL}(\mathbf{k})$, such that $m = \langle \Psi^\dagger M \Psi \rangle \neq 0$. Therefore, M s represent mass matrices. Such condition is satisfied only when

$$M = -(\sigma_1 \otimes \mathbb{I}_4) M^\top (\sigma_1 \otimes \mathbb{I}_4), \quad (27)$$

where \mathbb{I}_4 is a four dimensional identity matrix. There exists a unitary matrix $U = U_2 \otimes \mathbb{I}_4$ such that $\tilde{M} = -\tilde{M}^\top$, where $\tilde{M} = U M U^\dagger$ and

$$U_2 = \sqrt{\pm i} e^{i\frac{\pi}{4}\sigma_3} e^{i\frac{\pi}{4}\sigma_2} e^{i(\frac{\pi}{4}-\phi)\sigma_3}. \quad (28)$$

Therefore, after the unitary transformation all mass matrices are purely *imaginary* [5, 6].

Let us now write two mutually anticommuting four dimensional matrices, appearing in $H_0(\mathbf{k})$ as

$$\alpha_j = \Re(\alpha_j) + i \Im(\alpha_j), \quad (29)$$

for $j = 1, 2$. After such decomposition the kinetic energy of a DLSM assumes the form

$$H_{DL}(\mathbf{k}) = [\sigma_3 \otimes \Re(\alpha_1) + i\sigma_0 \otimes \Im(\alpha_1)] d_1(\mathbf{k}) + [\sigma_0 \otimes \Re(\alpha_2) + i\sigma_3 \otimes \Im(\alpha_2)] d_2(\mathbf{k}). \quad (30)$$

Since $U_2 \sigma_3 U^\dagger = \sigma_2$, after the unitary transformation with U the kinetic energy becomes

$$\tilde{H}_{DL}(\mathbf{k}) = [\sigma_2 \otimes \Re(\alpha_1) + i\sigma_0 \otimes \Im(\alpha_1)] d_1(\mathbf{k}) + [\sigma_0 \otimes \Re(\alpha_2) + i\sigma_2 \otimes \Im(\alpha_2)] d_2(\mathbf{k}) = \tilde{\Gamma}_1 d_1(\mathbf{k}) + \tilde{\Gamma}_2 d_2(\mathbf{k}). \quad (31)$$

Thus, $\tilde{\Gamma}_1$ and $\tilde{\Gamma}_2$ are respectively mutually anticommuting, but purely imaginary and real eight dimensional Hermitian matrices. We are after find all purely imaginary matrices (\tilde{M}) that anticommutes with $\tilde{\Gamma}_1$ and $\tilde{\Gamma}_2$. Since, $i\tilde{\Gamma}_1$ and $i\tilde{M}$ are purely imaginary and square to -1 , while $\tilde{\Gamma}_2$ is purely real and squares to $+1$, we seek to know maximal number of q so that for $p \geq 1$, the dimensionality of real matrices is eight and together they close $C(p, q)$ algebra. Notice that $C(p, q)$ Clifford algebra is defined by a set of $p + q$ mutually anticommuting matrices, among which p of them squares to $+1$, while q of them squares to -1 . The answer is $q = 4$ and $p = 1$ [7]. Thus maximal number of mutually anticommuting matrices is 5, and we define a set of such five matrices as $\{R, I_1, I_2, I_3, I_4\}$, where R is real and I_j s are imaginary for $j = 1, \dots, 4$. Two of those five matrices, say R and I_1 , can be used to define the kinetic energy. Therefore, I_2, I_3 and I_4 represents three mass matrices that together close a $Cl(3)$ algebra.

Pairing	available in	Spin structure	Spectrum
Δ_0	DLSM	singlet	$E_\alpha(\mathbf{k}) = \pm \left[d_1^2(\mathbf{k}) + d_2^2(\mathbf{k}) + \Delta_0^2 + \mu^2 - 2\alpha\sqrt{\mu^2(d_1^2(\mathbf{k}) + d_2^2(\mathbf{k})) + \Delta_0^2 d_2^2(\mathbf{k})} \right]^{1/2}$
Δ_s	DLSM	singlet	$E_\alpha(\mathbf{k}) = \pm \left[\left(\sqrt{d_1^2(\mathbf{k}) + d_2^2(\mathbf{k})} - \alpha\mu \right)^2 + \Delta_s^2 \right]^{1/2}$
Δ_2	DLSM	singlet	$E_\alpha(\mathbf{k}) = \pm \left[d_1^2(\mathbf{k}) + d_2^2(\mathbf{k}) + \Delta_0^2 + \mu^2 - 2\alpha\sqrt{(\mu^2 + \Delta_2^2)[d_1^2(\mathbf{k}) + d_2^2(\mathbf{k})]} \right]^{1/2}$
Δ_t	DLSM	triplet	$E_\alpha(\mathbf{k}) = \pm \left[d_1^2(\mathbf{k}) + d_2^2(\mathbf{k}) + \Delta_t^2 + \mu^2 - 2\alpha\sqrt{\mu^2(d_1^2(\mathbf{k}) + d_2^2(\mathbf{k})) + \Delta_t^2 d_1^2(\mathbf{k})} \right]^{1/2}$
Δ_W	WLSM	singlet	$E_\alpha(\mathbf{k}) = \pm \left[d_1^2(\mathbf{k}) + d_2^2(\mathbf{k}) + \Delta_W^2 + \mu^2 - 2\alpha\sqrt{\mu^2(d_1^2(\mathbf{k}) + d_2^2(\mathbf{k})) + \Delta_W^2 d_2^2(\mathbf{k})} \right]^{1/2}$

TABLE II: Quasiparticle spectrum within the mean field approximation in the presence of various local pairing in DLSM and WLSM, where $\alpha = \pm$. Each branch is two fold Kramers degenerate in DLSM, while Kramers degeneracy is absent in WLSM.

The Clifford algebra $C(1, 4)$ follows the quaternionic representation that supports *three* real Casimir operators, K_j for $j = 1, 2, 3$, besides the standard identity matrix. The Casimir operators satisfy the quaternionic algebra

$$K_i K_j = -\delta_{ij} + \epsilon_{ijk} K_k, \quad (32)$$

where δ_{ij} is the Kronecker delta function. From the casimir operators we can define imaginary matrices $E_j = iK_j$ for $j = 1, 2, 3$ and E_j s satisfy the $SU(2)$ algebra [6]. Notice that E_j s are purely imaginary Hermitian matrices that commute with $H_{DL}(\mathbf{k})$. From these three matrices we can define yet another set of three mutually anticommuting matrices $M'_j = iE_j R I_1$ that together close a $Cl(3)$ algebra and also anticommute with $H_{DL}(\mathbf{k})$. Hence, there are all together six purely imaginary matrices (thus mass) that anticommute with $H_{DL}(\mathbf{k})$ and they can be arranged into two sets according to

$$\{I_2, I_3, I_4\} \quad \text{and} \quad \{M'_1, M'_2, M'_3\}$$

that close a $Cl(3) \times Cl(3)$ algebra, as we announced in the main part of the paper.

• **Quasiparticle spectrum in the presence of pairings:** Finally we discuss the quasiparticle spectrum when pairing orders develop in a DLSM and WLSM. As discussed in the main part of the paper, a DLSM supports a fully gapped *s*-wave pairing. DLSM also supports various other singlet and triplet pairings that does not led to fully gapped quasiparticle spectrum. The effective single particle Hamiltonian in the presence of all possible local pairings in DLSM reads as

$$H_{SC}^{DLSM} = (\eta_1 \cos \phi + \eta_2 \sin \phi) \otimes (\Delta_0 \Gamma_0 + \Delta_s \Gamma_1 + \Delta_2 \Gamma_2 + \Delta_t [\vec{\sigma} \otimes \tau_3]), \quad (33)$$

where ϕ is the superconducting phase. On the other hand, a WLSM supports only one local pairing and in the presence of such local pairing effective single particle Hamiltonian is given by

$$H_{SC}^{WLSM} = (\eta_1 \cos \phi + \eta_2 \sin \phi) \otimes (\Delta_W \tau_0). \quad (34)$$

Quasiparticle spectrum in the presence of these pairings is shown in Table II.

In the presence of the singlet pairing [one with the amplitude Δ_0 in Eq. (33)] the spectrum of BdG fermions supports a pair of nodal rings at $k_z = \pm\sqrt{\Delta_0^2 + \mu^2}/v_z$, symmetrically placed about the $k_z = 0$ plane, with its radius being identical to the one in the normal state $k_\perp = k_F$. Consequently, a surface perpendicular to the (0,0,1) directions supports two degenerate circular flat bands of Andreev bound state with radius k_F (drumhead surface states). With increasing chemical potential (μ) or lowering the temperature below T_c , pairing amplitude increases monotonically and two thermal LNSM separate further in the reciprocal space.

With an underlying singlet *s*-wave pairing (with amplitude Δ_s) the quasiparticle spectrum is always fully gapped. Such singlet pairing thus represents a Majorana mass for nodal quasiparticles in a DLSM.

The triplet pairing [one with amplitude Δ_t in Eq. (33)] also supports two nodal ring in the paired phase. However, they are located in the $k_z = 0$ plane, with radii $k_\perp^\pm = [k_F^2 \pm 2m\sqrt{\Delta_0^2 + \mu^2}]^{1/2}$. The surface Andreev bound state perpendicular to (0,0,1) direction is comprised of two flat bands, representing the shadows of bulk line nodes. Thus,

as the temperature is gradually lowered below the transition temperature (T_c) or the chemical potential is gradually increased, the radius of one ring increases, while that for the other ring decreases continuously.

The remaining singlet pairing in DLSM [one with amplitude Δ_2 in Eq. (33)] gives rise to *four* nodal rings, discussed above. Since the condensation energy gain in the presence of four nodal rings are much less than that in the presence of a fully gapped pairing or nodal pairing that supports two thermal LNSM, we believe that such singlet pairing is energetically inferior.

The only local pairing in a WLSM produces a pair of nodal rings located at $k_z = \pm\sqrt{\Delta_W^2 + \mu^2}/v_z$ planes and their radii $k_\perp = k_F$ are identical. Thus with increasing μ or decreasing temperature below T_c , separation of two rings increases.

Appearance of any nodal superconductor (supporting thermal LNSM inside the ordered phase) at low temperatures can be detected from the measurement of specific heat (C_v), for example. Assuming that the pairing takes place in the vicinity of the Fermi surface, we expect C_v/T to be roughly constant, at least when temperature $T \ll E_F/k_B$ but $T > T_c$, where E_F is the Fermi energy. Inside the superconducting phase ($T < T_c$) $C_v \sim T^2$, yielding $C_v/T \sim T$ due to linear density of states arising from gapless BdG quasiparticles residing around the nodal rings. Since, $\varrho(\varepsilon) \sim |\varepsilon|$, ballistic BdG fermion becomes unstable toward the formation of a diffusive Majorana metal for infinitesimal amount of impurity [10, 11]. Thus, inside the paired state once again C_v/T becomes constant as $T \rightarrow 0$.

-
- [1] K. Gotfried and T-M. Yan, *Quantum Mechanics: Fundamentals*, 2nd ed., (Springer, 2004).
 - [2] H. B. Nielsen and M. Ninomiya, Nucl. Phys. **185**, 20 (1981).
 - [3] P. Hosur, S. Ryu, and A. Vishwanath, Phys. Rev. B **81**, 045120 (2010).
 - [4] I. F. Herbut, Phys.Rev.B **83**, 245445 (2011).
 - [5] A. Altland and M. R. Zirnbauer, Phys. Rev. B **55**, 1142 (1997).
 - [6] I. F. Herbut, Phys. Rev. B **85**, 085304 (2012).
 - [7] S. Okubo, J. Math. Phys. **32**, 1657 (1991).
 - [8] T. Senthil, and R. Shankar, Phys. Rev. Lett. **102**, 046406 (2009).
 - [9] Co-dimension d_c = physical dimension (d) - dimensionality of the hyperplane over which energy gap vanishes. Hence, for a d -dimensional Fermi surface $d_c = d - (d - 1) = 1$ and for a Fermi point system $d_c = d - 0 = d$. For a three dimensional LNSM $d_c = d - 1 = 2$.
 - [10] P. Goswami, and A. H. Nevidomskyy, Phys. Rev. B **92**, 214504 (2015).
 - [11] S. Bera, J. D. Sau, and B. Roy, Phys. Rev. B **93**, 201302(R) (2016).